Asian Journal of Chemistry; Vol. 31, No. 12 (2019), 2995-3003

ASIAN JOURNAL OF CHEMISTRY

https://doi.org/10.14233/ajchem.2019.22368

Fabrication of $MgFe_2O_4$-ZnO Nanocomposites for Photocatalysis of Organic Pollutants under Solar Light Radiation

KRUSHITHA SHETTY[1], B.S. PRATHIBHA[2,*], DINESH RANGAPPA[1], K.S. ANATHARAJU[3,*], H.P. NAGASWARUPA[4] and S.C. PRASHANTHA[4]

[1]Department of Nanotechnology, Visvesvaraya Technological University, P.G. Center, Muddenahalli, Chikkaballapur-562103, India
[2]Department of Chemistry, B.N.M. Institute of Technology, Bangalore-560070, India
[3]Department of Chemistry, Dayanand Sagar College of Engineering, Kumaraswamy Layout, Bangalore-560078, India
[4]Research Center, Department of Science, East West Institute of Technology, Bangalore-560091, India

*Corresponding authors: E-mail: pratbnmit@gmail.com; iamananthkurupalya@gmail.com

Received: 1 August 2019; *Accepted*: 16 September 2019; *Published online*: 16 November 2019; AJC-19653

$MgFe_2O_4$, ZnO and $MgFe_2O_4$-ZnO samples were successfully prepared through low temperature solution combustion route. The structural and morphological investigation were accomplished by PXRD, HRSEM, UV-visible and FTIR. The PXRD results point towards the reduced size of synthesized nanocomposites, which was further confirmed by HRSEM studies. Optical properties of the prepared samples were examined by UV-visible spectroscopy. The band gap seems to be widened for prepared nanocomposites compared to pure $MgFe_2O_4$. The photocatalytic degradation of methylene blue under sunlight was superior in contrast to pure $MgFe_2O_4$ and ZnO. $MgFe_2O_4$-ZnO (1:1) acts as the most effective photocatalyst activity compared to pure $MgFe_2O_4$ and ZnO. EIS data was proven to be an efficient tool for understanding the electronic properties for photocatalytic studies. The enhanced sunlight-driven photocatalytic activities of $MgFe_2O_4$-ZnO nanocomposite is supported by the factors such as quantization effect, band gap widening and efficient charge separation. $MgFe_2O_4$-ZnO showed excellent reusability with high photocatalytic efficiencies suggesting its suitability for solar photocatalytic applications. Additionally, scavenging test was conducted to know the role of all active species during photoelectrocatalysis. This work presents a facile and effective route for the construction of $MgFe_2O_4$-ZnO nanocomposites with intriguing structures and multiple functions.

Keywords: $MgFe_2O_4$-ZnO, Photoelectrocatalysis, Photoluminescence, Electrochemical activity.

INTRODUCTION

$MgFe_2O_4$ has a normal spinel structure AB_2O_4 with a tetrahedral A site and an octahedral B site occupied by Mg^{2+} ions and Fe^{3+} ions, respectively. The distribution of cations in the lattice sites defines the type of spinel structure [1]. It is noteworthy that some spinel ferrites, including $MgFe_2O_4$, are a class of semiconductors with narrow band gap. Spinel ferrites revealed that properties such as favourable magnetism, good photochemical stability, as well as excellent visible-light response [2,3]. These materials exhibit unique properties which have opened up a challenging gate for applications in photocatalytic process. Due to their poor property in photoelectric conversion and lower valence band potential, these ferrites can be used as photocatalysts [4]. Additionally, spinel ferrites possess noteworthy properties, such as superior chemical stability, enhanced mechanical hardness and high electrical resistivity [5].

$MgFe_2O_4$ has been investigated in-depth in the field of energy storage and conversion, due to outstanding magnetic and photoelectric property [6]. $MgFe_2O_4$ can respond to both ultraviolet and visible light, due to its small band gap which makes it became a kind of potential matrixes for preparing photocatalysis. Unfortunately, the disadvantage resulting from the fast recombination of photogenerated charges cause the non-ideal photocatalytic activities of bare $MgFe_2O_4$ for degradation or hydrogen production [7,8]. The visible light photocatalysis can be enhanced by coupling wide band gap material such as ZnO with the low band gap material such as $MgFe_2O_4$. By doing so, the photo-generated electrons and holes are well separated. ZnO has the wide band gap and its own unique property towards photocatalytic activity. In order to obtain the efficient

band gap that supports the effective degradation of dye, ZnO is combined with ferrite. Therefore, combinations of $MgFe_2O_4$ and ZnO nanophases to form nanocomposites are expected to provide new materials with multiple properties that effectively improved the utilization ratio of solar and repressed the recombination of photogenerated charge. Especially, it has been demonstrated in photocatalyst that diode structures which are made of narrow band gap semiconductors and broad band gap semiconductors show greatly enhanced activities compared with photocatalysts consisting of a single semiconductor.

Various synthesis routes are employed for the preparation of ferrite composites, such as sol-gel method, mechano-chemical, co-precipitation and microemulsion [9-12]. In the present work, the samples were prepared by solution combustion synthesis, which is well preferred for the synthesis of nanoparticles due to the voluminous yield, consumes less time, uniformly heating the reaction mixture and rapid reaction rates [13]. The fuel used here was environmentally friendly citric acid instead of oxalyl dihydrazide or urea that leads to toxic byproducts during synthesis.

In order to sustain the cost effective photocatalytic process, magnetic separation have been found to offer a convenient process for removing and recycling magnetic particles/composites by applying the external magnetic field. This method offers to prevent the agglomeration and sedimentation of the photocatalyst particles during the recovery stage, and thus can enhance the durability of the photocatalyst in the consequent treatment process.However, to our best of knowledge; there are few literatures about the preparation of $MgFe_2O_4$-ZnO nanocomposites and their use as photocatalysts. So, it seems essential to examine $MgFe_2O_4$-ZnO nanocomposites and their applications as magnetically separable photocatalysts.

Today′s society, pollution has gradually become a serious problem, particularly for water pollution, which is mainly caused by harmful chemical dyes such as methylene blue. Methylene blue is a harmful dye that can slowly cause physiological system disorders of human body. The present work is focused on the synthesis of $MgFe_2O_4$-ZnO nanocomposites in different ratios *via* solution combustion synthesis and to study the photocatalytic activity for the degradation of methylene blue dye under sunlight. The optical band gap of prepared samples is investigated. The electrochemical property is discussed with the help of electrochemical instrument spectroscopy. The enhancement of photoelectrochemical properties are correlated with the photocatalytic activity. The stability of prepared photocatalyst is examined and reported. This can be attributed to the formation of $MgFe_2O_4$ heterostructure, which effectively improved the utilization ratio of solar and repressed the recombination of photo-generated charge. In order to evaluate its longevity in photocatalytic performance, the magnetically-assisted separation technique was employed to retrieve this nanocomposite and a sequential recyclability test was conducted.

EXPERIMENTAL

Synthesis of $MgFe_2O_4$ and ZnO nanoparticles: All the chemicals used in present work for the synthesis were procured from Merck, India. $MgFe_2O_4$ nanoparticles were synthesized by mixing calculated proportions of magnesium nitrate and ferric nitrates with a certain amount of citric acid as fuel. ZnO nanoparticles were also prepared using zinc nitrate and citric acid. The mixture of precursors and fuel were added with 10 mL of distilled water and kept for stirring to obtain homogeneous mixture. After few min, the mixture is placed in the pre-heated muffle furnace at 500 ± 10 ºC. Initially, water molecules evaporated and the mixture gradually caught fire at one corner that spread through entire mass ensuring the complete combustion resulted in a fluffy and voluminous yield in the container. The as-synthesized products were used for further use.

Synthesis of $MgFe_2O_4$-ZnO nanocomposites: Three variant of $MgFe_2O_4$-ZnO nanocomposites were prepared with molar concentrations of $MgFe_2O_4$:ZnO as 1:1, 1:2 and 2:1. Stochiometry amount of magnesium nitrate and zinc nitrate, ferric nitrate were used as oxidizing materials and citric acid as fuel for the preparation $MgFe_2O_4$-ZnO nanocomposites and followed the procedure that was used for the synthesis of $MgFe_2O_4$ and ZnO nanoparticles.

Characterization: The structural and composition analysis of $MgFe_2O_4$, ZnO and $MgFe_2O_4$-ZnO were accomplished by following technical methods. Powder X-ray diffraction (PXRD) was run with PAN alytical X'Pert Pro utilizing CuKα radiation with a scanning speed at 2θ of 2º min^{-1}. The scanning electron microscope images (JOEL JSM 840 A) were obtained by sputtering system with gold as encasing contrast materials. The infrared spectra were recorded by Perkin-Elmer FTIR spectrometer, (spectrum 1000) device. DRS spectra were recorded by Shimadzu UV-300 spectrophotometer equipped with integrating sphere appliance. The absorption spectra are recorded by UV-Vis spectrophotometer (SL 159, ELICO).

RESULTS AND DISCUSSION

XRD analysis: The phase purity for $MgFe_2O_4$, ZnO and $MgFe_2O_4$-ZnO was verified from PXRD analysis. The diffraction peaks at 30.36º, 35.77º, 43.35º, 53.88º, 57.03º and 62.83º correspond to $MgFeFe_2O_4$ nanoparticles with cubic spinel structure (JCPDS73-1720) (Fig. 1). Moreover, all diffraction peaks in pattern (Fig. 1) were indexed to (100), (002), (101), (102), (110), (103), (200), (112) and (201) planes of ZnO wurtzite structure (JCPDS No: 36-1451) and no extra phase were observed indicating single phase of prepared samples. The narrow peaks of ZnO represent the high crystalinity of particles. Peaks for both $MgFe_2O_4$ and ZnO were seen in the PXRD patterns for different ratios of $MgFe_2O_4$-ZnO nanocomposites. The peaks were broad for $MgFe_2O_4$-ZnO nanocomposites compared to host particles approving small crystalline size of nanocomposites. The sharp peaks of host $MgFe_2O_4$ and ZnO approve high crystallinity of nanoparticles. The crystallite size was found using Debye-Scherrer′s relation [14] and structural parameters are tabulated in Table-1.

Morphology analysis: Fig. 2a shows the SEM image of $MgFe_2O_4$ which has agglomerated spinel particles with voids and pores. The image for 1:1 $MgFe_2O_4$-ZnO nanocomposite shows little spongy natured spinels in Fig. 2b, while Fig. 2c illustrates the SEM image of 1:2 $MgFe_2O_4$-ZnO nanocomposite. The sample is spongier with less aggregation and Fig. 2d shows the SEM image of 2:1 $MgFe_2O_4$-ZnO nanocomposite,

TABLE-1
PARTICLE SIZE, DISLOCATION DENSITY AND STACKING FAULT FOR $MgFe_2O_4$, ZnO AND $MgFe_2O_4$-ZnO SAMPLES

Samples	FWHM	Crystalline size (nm)	SF × 10^{-3}	δ (10^{15} lin m^{-2})
$MgFe_2O_4$	0.4201	22.3	0.3912	1.8284
ZnO	0.678	20.0	0.4470	6.94
1:1 $MgFe_2O_4$-ZnO	0.5992	16.77	0.3899	3.555
1:2 $MgFe_2O_4$-ZnO	0.6291	17.0	0.3887	3.427
2:1 $MgFe_2O_4$-ZnO	0.5846	20.2	0.3899	2.4507

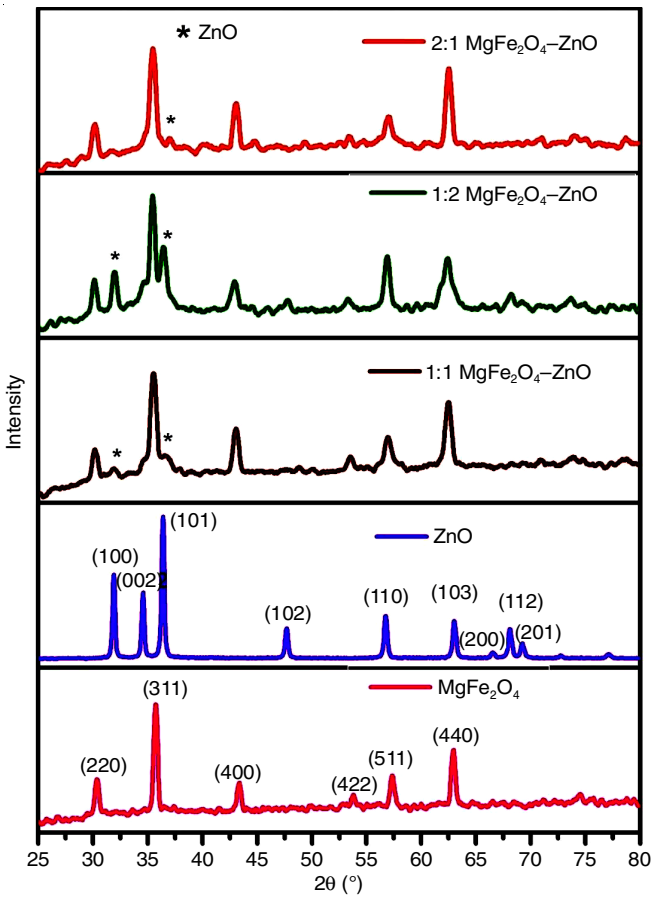

Fig. 1. PXRD paterens for prepared nanoparticles

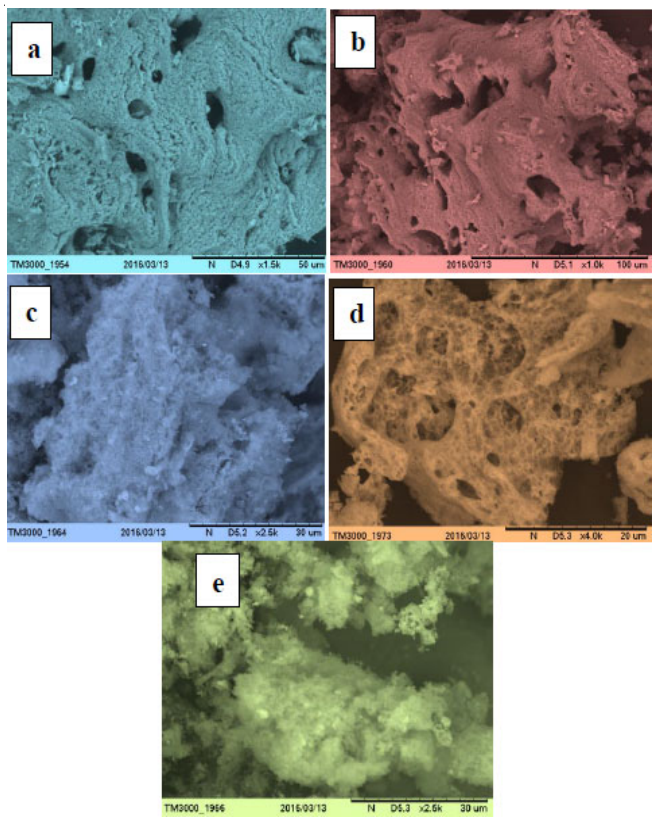

Fig. 2. SEM images of (a) $MgFe_2O_4$, (b) 1:1$MgFe_2O_4$-ZnO, (c) 1:2 $MgFe_2O_4$-ZnO, (d) 2:1 $MgFe_2O_4$-ZnO, (e) ZnO

where both spongy nature as well as spinel formation can be observed clearly. It was observed that as the ferrite content increases, the agglomeration of particles was also increased. ZnO particles exhibited spongy nature with fragile network (Fig. 2e).

FTIR analysis: Fig. 3 displays FTIR spectra of as- prepared samples range from 4000 to 400 cm^{-1}. Around 750 and 490 cm^{-1}, the stretching vibration of octahedral and tetrahedral sites leads to two main peaks respectively signifying the formation of spinel ferrite [15]. A peak at 465 cm^{-1} can be seen near the band ν_2 at 490 cm^{-1}. This band arise may be because of Jahn-Teller distortion introduced by Fe^{2+} ions [16]. The weak shoulder of bands in $MgFe_2O_4$-ZnO refers to existence of ZnO in the sample. However, the presence of absorbed water in the samples leads to H-O-H bending vibration and stretching modes resided at 3465.80 cm^{-1} [17]. The variation in the position and intensity in the FTIR spectra of nanocomposite results due to presence of change in the ratios of Zn^{2+} ions with the respective nano-composites. In present research, highest band locates at 750 cm^{-1} and corresponds to intrinsic stretching vibrations of metal

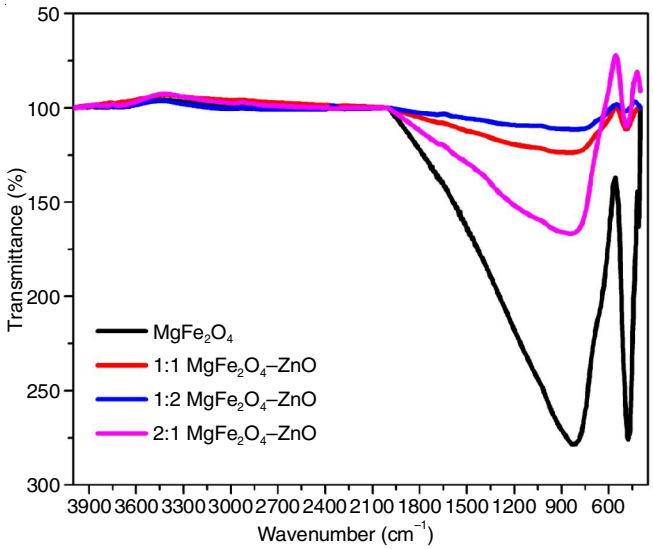

Fig. 3. FTIR spectra for prepared nanoparticles

at the tetrahedral site. Whilst lowest band appears at 490 cm^{-1} assigns to octahedral-metal stretching.

UV-Vis-DRS study and calculation of band gap: UV-vis spectroscopy was used to find the optical property of the prepared samples. Due to light absorption property and the vital role towards the photocatalytic activity of synthesized samples necessitate to check the band-gap for each prepared samples. Kubelka-Munk function is used to verify the band gap:

$$\alpha = 1–R^2/2R \quad (1)$$

$$(\alpha h\nu)^2 = B\ (h\nu – Eg)n \quad (2)$$

where hν is the photon energy, α is the absorption coefficient, B is a constant. Kubelka Munk function was plotted as the function of absorption energy to find the band gap.

By extrapolating the straight line to the axis x = 0, the band-gap was determined. Fig. 4 shows the plot for all the synthesized samples. In the range of wavelength between 500 and 600 nm a sharp increase in peak is observed. As shown in Fig. 4, the addition of Zn content in sample resulted in the red shift of band-gap adsorption edge and also increases in the intensity compared to pure $MgFe_2O_4$. This indicates the presence of quantization effect and size reduction. As ZnO content is increased, the band gap adsorption edge increases indicating the bandgap for 1:1 $MgFe_2O_4$-ZnO,1:2 $MgFe_2O_4$-ZnO and 2:1 $MgFe_2O_4$-ZnO were 2.43, 2.49, 2.38 nm, respectively. The band gap for $MgFe_2O_4$ and ZnO was 2.3 and 2.65 nm, respectively. The ZnO formation in the nanocomposite is the reason for the rise in band gap of all the synthesized nanocomposites.

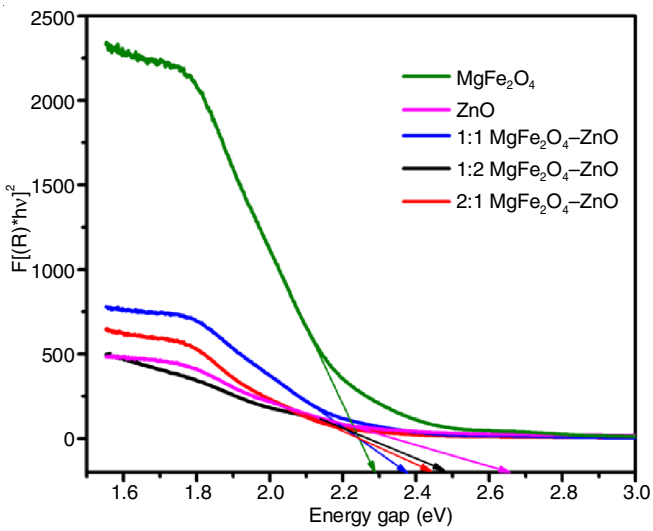

Fig. 4. Band gap graph for prepared nanoparticles

Photoluminescence study: Tuning the band structure in a photocatalyst is basically to delay or decrease the recombination possibilities during the photocatalytic process. Fig. 5 displays the photoluminescence (PL) spectra of synthesized samples at various loading amounts of ZnO in the wavelength range of 300-500 nm after the excitation at 372 nm. As can be clearly seen in emission spectra nanocomposites show drastically reduced luminescence peaks although their shapes and positions are not virtually changed. The decrease in the intensity with addition of ZnO content, suggests the decreasing number of optically active centres due to quenching effect. In the deep level luminescence band, all the samples display a defectrelated visible luminescence band, which is usually related to the defects, such as interstitial defects and oxygen vacancies [18].

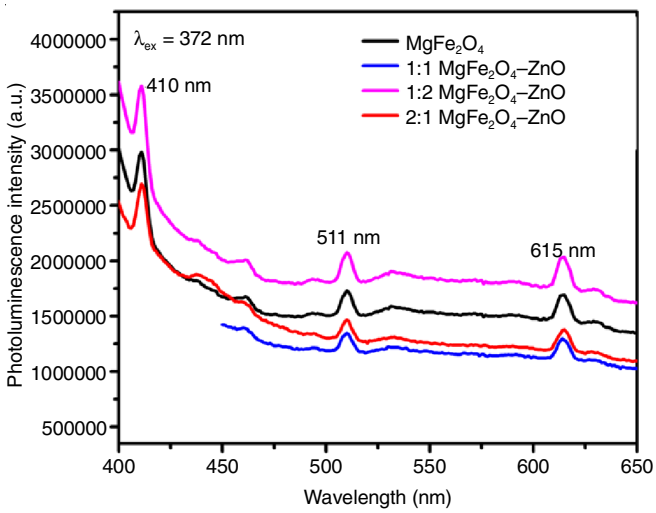

Fig. 5. Photoluminescence spectra for prepared samples

The photoluminescence spectra of all the samples show the major peak at 510 nm, which is mainly attributed radiative emission of mesoporous nanostructures during recombination of electrons and holes, while emission at 410 and 614 nm are due to donor-acceptor interactions, the recombination owing to the defects and impurity components. It should be noted that photoluminescence intensity of the major signal at 510 nm is greatly reduced for all nanocomposites. The significance of photoluminescence spectra is to study the nature of electron-hole pairs on immigration, trapping and transfer properties [19]. Since, the emission signal at 510 nm driven from the recombination of excited electron-hole pair, the fall in photoluminescence intensity is well related to the improved recombination resistance due to the delocalization of excited electrons in the conduction band. Hence, itsignifies that 1:1 $MgFe_2O_4$-ZnO nanocomposite may revealed better photocatalytic activity in comparison to the other nanocomposites to degrade the dye. On the other hand, a weak photoluminescence peak of 1:1 $MgFe_2O_4$-ZnO, which might result from the enhanced electron-phonon interactions (polaronic effect) was observed by Zhang *et al.* [20,21].

Commonly colour of phosphor material can be depicted by Commission International De I-Eclairage (CIE) chromaticity coordinates. The CIE coordinates for $MgFe_2O_4$-ZnO phosphors was estimated with respect to ZnO concentration (Fig. 6a). The white and green emission was observed for $MgFe_2O_4$ and 1:1 $MgFe_2O_4$-ZnO, respectively. Other two phosphors (1:2 and 2:1 $MgFe_2O_4$-ZnO) exhibited blue emission as shown in Fig. 6a. The CIE coordinates of colour emission of Fe^{2+} ions not only rely upon the asymmetric ratio but also influenced by the higher energy emission levels. Hence, all $MgFe_2O_4$-ZnO nanocomposite exhibits different colour which depends on respective photoluminescence intensity [22].

To examine the colour quality of light emission and colour temperature, coordinated colour temperature (CCT) values were calculated for the present phosphors. CCT was calculated by converting the (x, y) coordinates of the light source to (U′′, V′′) based on following equations and by finding the temperature of the closest point of Planckian locus to the light source on (U′′, V′′) uniform chromaticity diagram (Fig. 6b) [23,24].

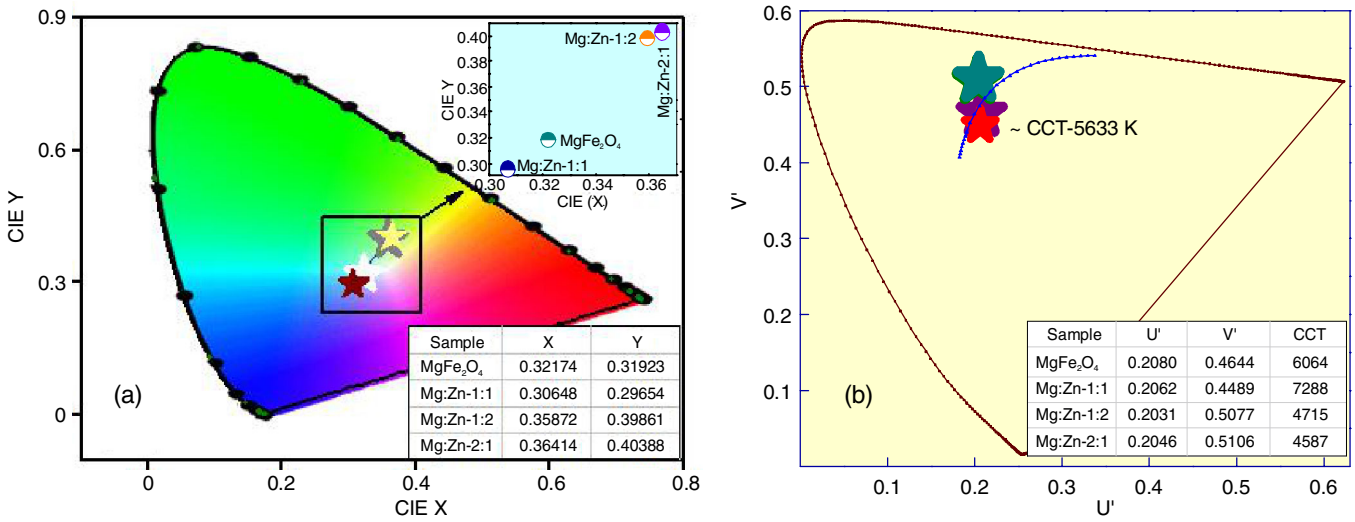

Fig. 6. (a) CIE and (b) CCT diagram for prepared nanoparticles

$$U'' = \frac{4x}{-2x + 12y + 3} \quad (3)$$

$$V'' = \frac{9y}{-2x + 12y + 3} \quad (4)$$

Coordinated colour temperature (CCT) is usually estimated by Planckian locus, *i.e.* a small part of (x, y) chromaticity diagram and outside the Planckian locus more operating points can be found. The CCT is used to determine the colour temperature of a light source, if the CCT coordinates of a light source do not intersect on the Planckian locus. The acquired CCT value is confirmed by theoretical CCT value as estimated by McCamy empirical formula:

$$CCT = -437\ n^3 + 3601\ n^2 - 6861\ n + 5514.31$$

where $n = (x - x_c)/(y - y_c)$ and was well matched with 5663 K.

The estimated CCT values is higher than 5000 K, which indicates that the present phosphors can be utilized for cool white light used in domestic appliances. These phosphors can be used in sold state display as well as LED applications.

Electrochemical impedance study: The electrochemical impedance spectroscopy was analyzed by CHI660 B electrochemical analyzer (CH Instruments, 0.01 Hz to100 kHz, with open circuit voltage for -0.4 V). The dynamics of charges in the bulk or interfacial region of semiconductor could be studied by solid-state impedance spectroscopy. The Nyquist plot is a standard format of evaluating the impedance data. EIS plot displayed an arc and a slanted line in the high frequency region and low frequency region respectively (Fig. 7). The diameter of arc for 1:1 $MgFe_2O_4$-ZnO was very less compared to other indicating the lower charge transfer resistance (R_{CT}) and faster separation of photogenerated charge would endow 1:1 $MgFe_2O_4$-ZnO nanocomposite with enhanced photochemical activity [25,26]. The charge transfer resistance values for 1:1, 1:2, 2:1 $MgFe_2O_4$-ZnO, $MgFe_2O_4$ and ZnO are 32,100, 92,50 and 180 Ω, respectively. The charge transfer resistance is related to Warburg resistance, which is the resistance to mass transfer and is governed by the specific conductance.

The large arc indicates that the possibility of more electrons to reach semi-conductor/electrolyte interface is very less compared to the photocatalyst that possesses small arc. Hence, during

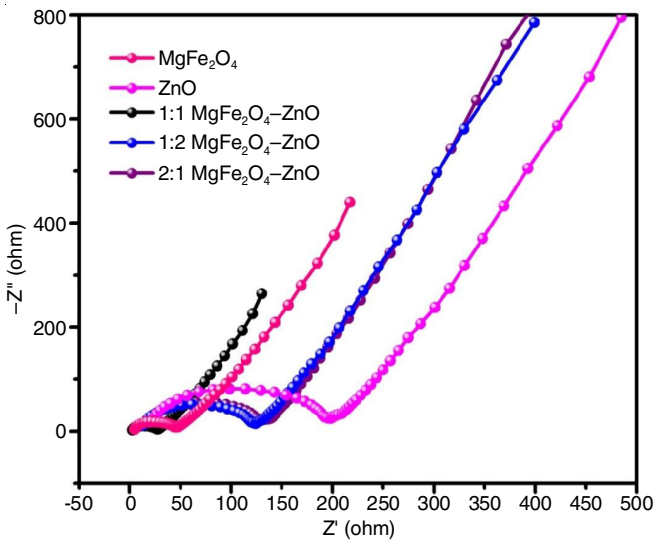

Fig. 7. EIS spectra for prepared nanoparticles

the photocatalysis these photocatalysts have more chance of recombining before reacting with pollutants. The enhanced photocatalytic activity of composite can be tackled to a lesser electron-hole recombination since lower R_{CT} leads efficient charge separation of electron/hole pairs and fast conduction until the surface to react with contaminants.Therefore, EIS results gave an important proof that the $MgFe_2O_4$-ZnO has effectively optimized the photoelectrochemical activities of bared electrodes.

Photocatalytic degradation of methylene blue under solar light irradiation: The photocatalysis was experimented on sunny days between 11 am and 2 pm in the month of May 2019 at Bangalore, India. The entire method has already been discussed in previously article [24]. To carry out the experiment, 20 mL of methylene blue dye solution were taken with 20 mg of prepared sample and added to 250 mL of deionized water and kept under sunlight. This dispersed solution was uniformly mixed using a magnetic stirrer during complete time span of experiment. The adsorption/desorption equilibrium can be achieved by stirring the reaction mixture for 30 min before irradiation. The absorbance of methylene blue solutions was measured with UV-visible absorption spectrophotometer (SL

159, ELICO) for each 15 min interval of time. Then, 5 mL aliquots were obtained at regular time intervals then immediately centrifuged and filtered through 0.45 μm Millipore filter to remove the catalyst particles. This becomes essential for the spectrophotometric analysis and in resolving residual concentration of methylene blue. The photocatalytic actions of these photocatalysts were estimated by using the measurement of absorbance of aqueous IC solution as a function of the irradiation time using an UV-Vis spectrophotometer (Shimadzu, UV-3150). Similar kind of control experiments was carried out with or without catalysts (blank) in dark conditions.

The degradation ability of each prepared samples were investigated. The absorption spectra for each sample are shown in Fig. 8. Fig. 9 shows the percentage degradation and with time for photodegradation of methylene blue. According to the obtained result, there was no much degradation of dye in the absence of light and in the presence of sunlight with no photocatalyst resulted a very negligible degradation of dye. Degradation ability of 1:1 $MgFe_2O_4$-ZnO was 96 % after 45 min. While 2:1 and 1:2 $MgFe_2O_4$-ZnO nanocomposites showed percentage degradation of 89 and 75 %, respectively. Pure $MgFe_2O_4$ and ZnO showed less degradation performance of 63 and 50 %, respectively. The enhanced photocatalytic activity of 1:1 $MgFe_2O_4$-ZnO may be attributed to the quantum size effect, and efficient band gap, defects in the grain boundaries due to hybridization of ZnO and $MgFe_2O_4$. It is clearly seen that the photodegradation efficiency of methylene blue increases initially with 1:1 $MgFe_2O_4$-ZnO concentration. This phenomenon may be attributed with increase in $MgFe_2O_4$ nanoparticles; the heterojunction area between $MgFe_2O_4$ and ZnO increases and more electron-hole pairs will separate under illumination, which is beneficial to degrading the organic dyes. The photodegradation efficiency of methylene blue then decreases as $MgFe_2O_4$ and ZnO concentration further increases. This phenomenon may be attributed to that more $MgFe_2O_4$ and ZnO deposition would cause conglomeration and growth of $MgFe_2O_4$ and ZnO nanoparticle catalysis, the electron jumps from valance band to conduction band. This hole-electron pair recombine very easily due to inefficient charge separation in pure $MgFe_2O_4$ and ZnO nanoparticles. Hence, it lessens the life span of excited electrons and holes thereby diminishing the photocatalytic performance under sunlight illumination. Whereas in nanocomposite, the excited electrons transfers from $MgFe_2O_4$ to ZnO because of more negative conduction offset of $MgFe_2O_4$ than ZnO. Further, the excited electrons react with atmospheric oxygen molecules and forms superoxide radicals. The left over holes in valence band combines with water and hydroxyl ions to form hydroxyl radicals. Highly reactive radicals react with methylene blue dye and decompose it into smaller organic compounds. The photocatalytic mechanism can be summarized in following reactions:

$$MgFe_2O_4\text{-}ZnO + Sunlight \longrightarrow (e^- + h^+)MgFe_2O_4\text{-}ZnO \quad (4)$$

$$MgFe_2O_4\text{-}ZnO\ (e^-) + O_2 \longrightarrow O_2^{\bullet -} \quad (5)$$

$$H_2O + h^+ \longrightarrow H^+ + OH^\bullet \quad (6)$$

$$(h^+)\ MgFe_2O_4\text{-}ZnO + OH^- \longrightarrow OH^\bullet \quad (7)$$

$$OH^\bullet + O_2^{\bullet -} + Dye \longrightarrow Degraded\ product \quad (8)$$

The degree of adsorption can be determined from the following equation:

$$Q = [(C_0 - C)V]/W \quad (9)$$

where Q = amount of adsorption (ppm mL mg^{-1}); C_0 and C = concentrations before and after adsorption, V = volume of the reaction mixture and W = amount of catalyst (g).

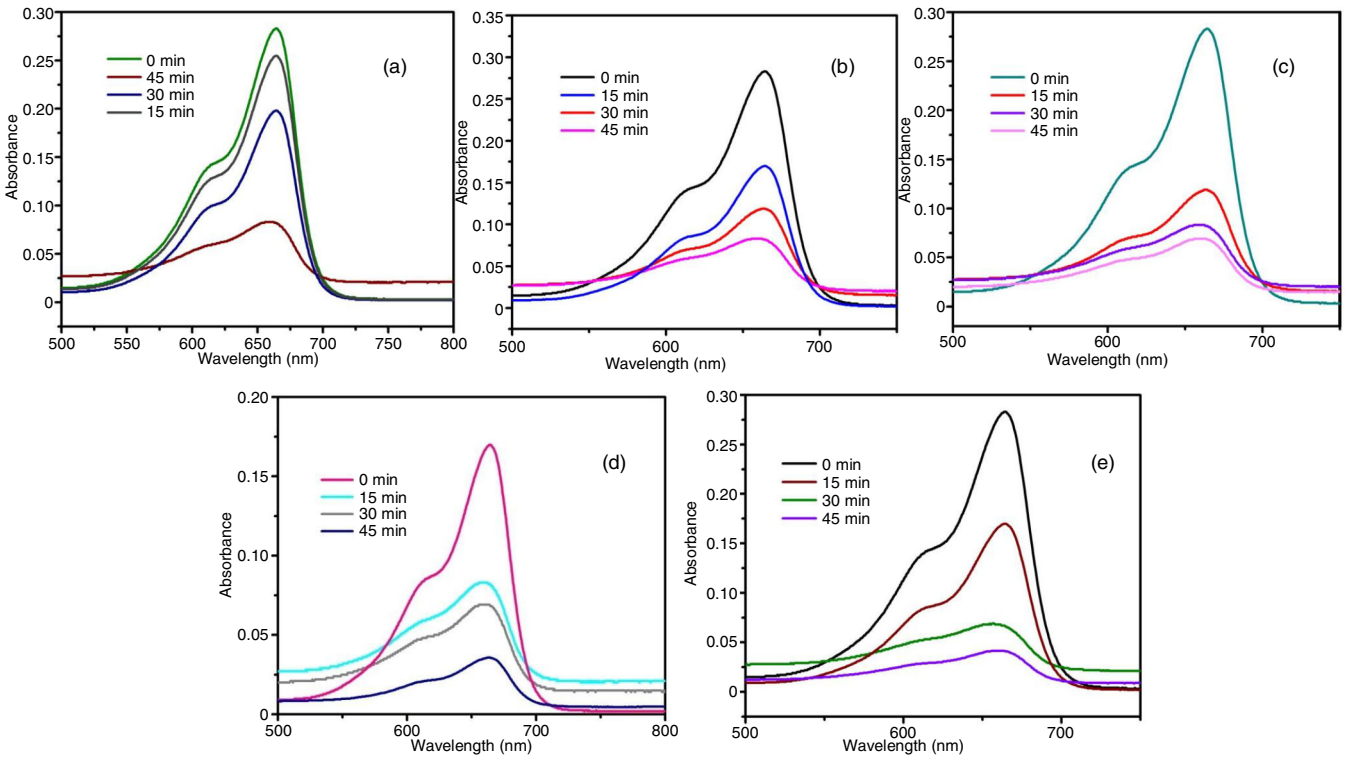

Fig. 8. Absorption spectra for prepared (a) ZnO, (b) $MgFe_2O_4$, (c) 1:2 $MgFe_2O_4$-ZnO, (d) 2:1 $MgFe_2O_4$-ZnO, (e) 1:1 $MgFe_2O_4$-ZnO

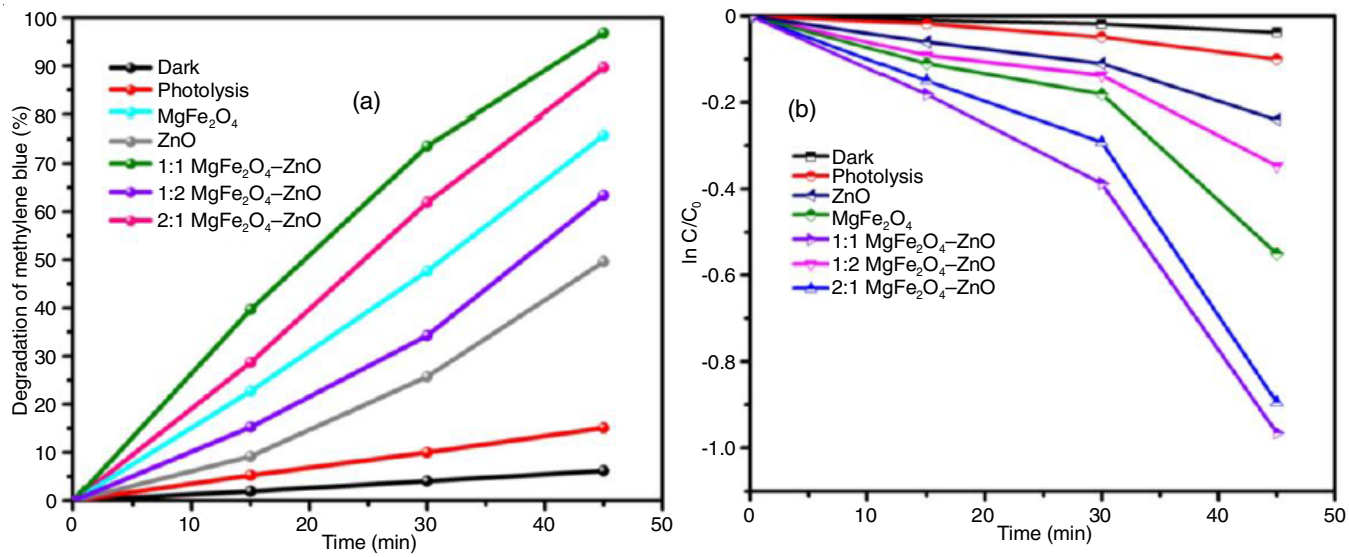

Fig. 9. ln C/C_0 spectra and percentage degradation for prepared nanoparticles

The photocatalyst 1:1 $MgFe_2O_4$-ZnO nanocomposite was tested for different types of dyes including lanasyn red (LR), malachite green (MG), rhodamine B (RB) and metanil yellow (MY) under sunlight illumination for about 45 min. The results showed that all the dyes have showed decomposition above 80 % (Fig. 10a), which proves the potentialability of synthesized photocatalyst.

One of the biggest problems for the photocatalysis of ZnO is it's photostability, which is related with crystallinity, charge transfer and others. Therefore, to be a good photocatalyst, it has to be stable and reusable. Recycling experiment was carried out to examine the stability of photocatalyst so that it can be used for practical applications. To reuse the photocatalyst from the reaction mixture an external bulk magnet is used [27]. The extracted photocatalyst was washed with ethanol and dried for each run. Further, the photocatalyst is used for the next 4 more runs for the degradation of methylene blue dye. At the end of experiment, photocatalyst is extracted again for the further run. The graph is plotted for all five runs with percentage degradation with respect (Fig. 10b). The results showed almost consistency in the decomposition rate for all the 5 runs ensuring the stability of photocatalyst.

The PXRD analysis was performed for 1:1 $MgFe_2O_4$-ZnO nanocomposite before and after photocatalytic experiment and the results are shown in Fig. 11. It was noted that after the photocatalytic experiment, no change was observed in the crystal structure of 1:1 $MgFe_2O_4$-ZnO and no secondary phase was observed. This gives the evidential proof for the stability of 1:1 $MgFe_2O_4$-ZnO nanocomposite.

Scavenging tests were used to check the photocatalytic efficiency of hyper active radicals in the degradation of dyes in the existence of 1:1 $MgFe_2O_4$-ZnO nanocomposite. To block the photogenerated h^+, during photocatalysis only 0.5 mM EDTA was made use of. This efficiently blocked h^+ ions and successfully avoided it by involving in the photocatalysis. As shown in Fig. 12, the degradation was precisely lessened in existence of ethanol. Additionally, for the subsequent experimentation, 0.5 mM silver nitrate was mixed to dye mixture. Silver nitrate blocked the photoelectrons in the process and the photodegradation reduced by 20 % confirming the blockage of photo-

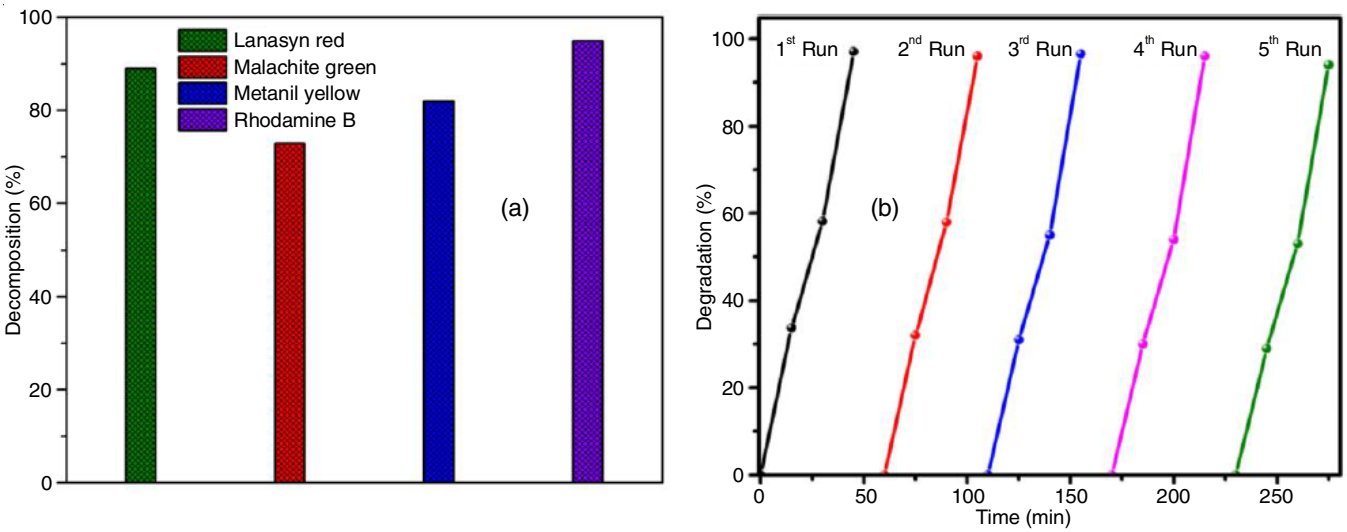

Fig. 10. (a) Percentage degradation of different dyes using 1:1 $MgFe_2O_4$-ZnO nanocomposite, (b) Recycling experiment for 1:1 $MgFe_2O_4$-ZnO nanocomposite

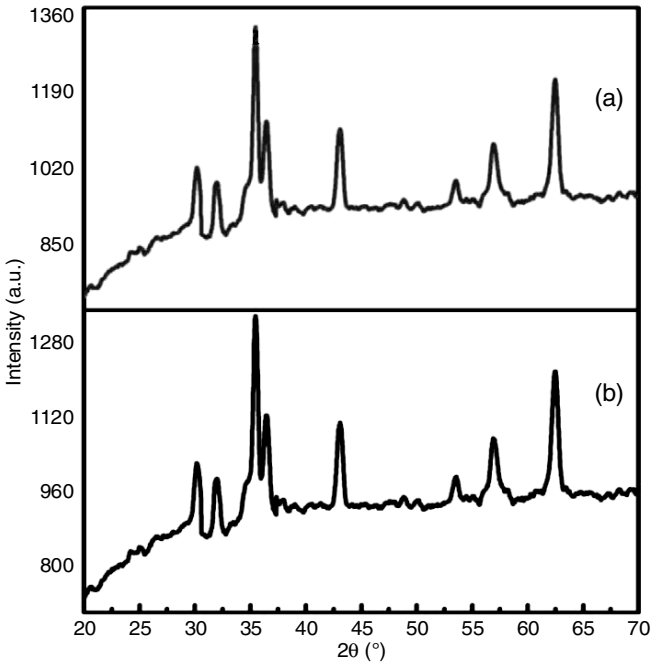

Fig. 11. PXRD of 1:1 $MgFe_2O_4$-ZnO nanocomposite (a) before and (b) after photocatalysis

electrons and permitting the h^+ to degradation of dye compound [28]. Fig 12 depicts the photodegradation of methylene blue in presence of scavengers. *tert*-BuOH (0.5 mM) is mixed to the reaction mixture to trap the $OH^•$, where the photodegradation activity changed slightly [29]. This ensures that photo-generated h^+ ions are the main concern for oxidation process in photocatalytic reaction. According to the attained scavenging test, h^+ ions are the mainly accountable for major degradation of dye compound. These photo-generated h^+ ions straightly counter with dye compound for the complete degradation.

Conclusion

In summary, $MgFe_2O_4$, ZnO and $MgFe_2O_4$-ZnO samples were synthesized effectively through by solution combustion route using citric acid as a fuel. The PXRD, HRSEM and FTIR confirmed the successful preparation of the desired samples. EIS results revealed the significant charge transfer rate and fast charge separation that contributed towards enhanced photocatalytic activity of the $MgFe_2O_4$-ZnO nanocomposites. In addition, the photodegradation process of the obtained samples and its possible reaction mechanism was proposed. Band gap widening, superior textural properties and efficient electron hole separation were identified as the factors responsible for the enhanced sunlight-driven photocatalytic activities of $MgFe_2O_4$-ZnO nanocomposites. Scavenging test also revealed that the mainly holes of $MgFe_2O_4$-ZnO nanocomposites contribute in the degradation of methylene blue under sunlight illumination. Synthesized nanocomposites were conveniently recovered and reused by using a magnet, which is favourable for realistic applications.

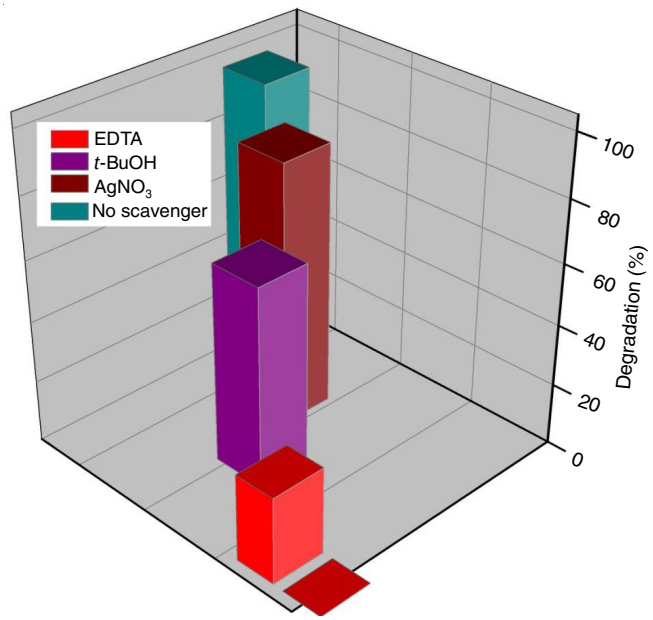

Fig. 12. Scavenging experiment for 1:1 $MgFe_2O_4$-ZnO nanocomposite

CONFLICT OF INTEREST

The authors declare that there is no conflict of interests regarding the publication of this article.

REFERENCES

1. G.Y. Zhang, C.S. Li, F.Y. Cheng and J. Chen, *Sens. Actuators B*, **120**, 403 (2007); https://doi.org/10.1016/j.snb.2006.02.034.
2. X.Y. Li, Y. Hou, Q.D. Zhao, W. Teng, X.J. Hu and G.H. Chen, *Chemosphere*, **82**, 581 (2011); https://doi.org/10.1016/j.chemosphere.2010.09.068.
3. P. Laokul, V. Amornkitbamrung, S. Seraphin and S. Maensiri, *Curr. Appl. Phys.*, **11**, 101 (2011); https://doi.org/10.1016/j.cap.2010.06.027.
4. S.H. Xu, D.L. Feng and W.F. Shangguan, *J. Phys. Chem. C*, **113**, 2463 (2009); https://doi.org/10.1021/jp806704y.
5. S.W. da Silva, T.F.O. Melo, M.A.G. Soler, E.C.D. Lima, A.F. da Silva and P.C. Morais, *IEEE Trans. Magn.*, **39**, 2645 (2003); https://doi.org/10.1109/TMAG.2003.815540.
6. J.C. Fu, J.L. Zhang, C.H. Zhao, Y. Peng, X.D. Li, Y.M. He, Z.X. Zhang, X.J. Pan, N.J. Mellors and E.Q. Xie, *J. Alloy. Compd.*, **577**, 97 (2013); https://doi.org/10.1016/j.jallcom.2013.04.177.
7. X.Z. Yuan, H. Wang, Y. Wu, X.H. Chen, G.M. Zeng, L.J. Leng and C. Zhang, *Catal. Commun.*, **61**, 62 (2015); https://doi.org/10.1016/j.catcom.2014.12.003.
8. H.G. Kim, P.H. Borse, J.S. Jang, E.D. Jeong, O.S. Jung, Y.J. Suh and J.S. Lee, *Chem. Commun.*, 5889 (2009); https://doi.org/10.1039/b911805e.
9. J.G. Lee, H.M. Lee, C.S. Kim and Y.J. Oh, *J. Magn. Magn. Mater.*, **177-181**, 900 (1998); https://doi.org/10.1016/S0304-8853(97)00925-6.
10. K. Maaz, A. Mumtaz, S.K. Hasanain and A. Ceylan, *J. Magn. Magn. Mater.*, **308**, 289 (2007); https://doi.org/10.1016/j.jmmm.2006.06.003.
11. R. Sani, A. Beitollahi, Y.V. Maksimov and I.P. Suzdalev, *J. Mater. Sci.*, **42**, 2126 (2007); https://doi.org/10.1007/s10853-006-1235-9.
12. Z.T. Zhang, A.J. Rondinone, J.X. Ma, J. Shen and S. Dai, *Adv. Mater.*, **17**, 1415 (2005); https://doi.org/10.1002/adma.200500009.
13. N. Deraz and E. Alarifi, *J. Anal. Appl. Pyrolysis*, **97**, 55 (2012); https://doi.org/10.1016/j.jaap.2012.04.006.
14. Y.S. Vidya, K. Gurushantha, H. Nagabhushana, S.C. Sharma, K.S. Anantharaju, C. Shivakumara, D. Suresh, H.P. Nagaswarupa, S.C. Prashantha and M.R. Anilkumar, *J. Alloy. Compd.*, **622**, 86 (2015); https://doi.org/10.1016/j.jallcom.2014.10.024.
15. N. M. Deraz and A. Alarifi, *J. Anal. Appl. Pyrolysis*, **97**, 55 (2012); https://doi.org/10.1016/j.jaap.2012.04.006.
16. V.A. Potakova, N.D. Zverv and V.P. Romanov, *Phys. Stat. Solid. (a)*, **12**, 623 (1972); https://doi.org/10.1002/pssa.2210120235.

17. V.K. Sankaranarayanan and C. Sreekumar, *Curr. Appl. Phys.*, **3**, 205 (2003); https://doi.org/10.1016/S1567-1739(02)00202-X.
18. S. Yilmaz, E. Bacaksiz, E. McGlynn, I. Polat and S. Ozcan, *Thin Solid Films*, **520**, 5172 (2012); https://doi.org/10.1016/j.tsf.2012.04.002.
19. S.A. Ansari, M.M. Khan, S. Kalathil, A. Nisar, J. Lee and M.H. Cho, *Nanoscale*, **5**, 9238 (2013); https://doi.org/10.1039/c3nr02678g.
20. B. Zou, W. Huang, M. Han, S. Li, X. Wu, Y. Zhang, J. Zhang, J. Zhang, P. Wu and R. Wang, *J. Phys. Chem. Solids*, **58**,1315 (1997); https://doi.org/10.1016/S0022-3697(97)00038-3.
21. Q. Han, Z. Liu, Y. Xu, Z. Chen, T. Wang and H.J. Zhang, *Phys. Chem. C*, **111**, 5034 (2007); https://doi.org/10.1021/jp067837m.
22. P.B. Devaraja, D.N. Avadhani, S.C. Prashantha, H. Nagabhushana, S.C. Sharma, B.M. Nagabhushana, H.P. Nagaswarupa and H.B. Premkumar, *Spectrochim. Acta A: Mol. Biomol. Spectrosc.*, **121**, 46 (2014); https://doi.org/10.1016/j.saa.2013.10.060.
23. D.B. Judd, *J. Opt. Soc. Am.*, **26**, 421 (1936); https://doi.org/10.1364/JOSA.26.000421.
24. K. Shetty, S.V. Lokesh, H.P. Nagaswarupa, H. Nagabhushana, D. Rangappa, K.S. Anantharaju, S.C. Prashantha, Y.S. Vidya and S.C. Sharma, *Physica B: Conden. Matt.*, **507**, 67 (2017); https://doi.org/10.1016/j.physb.2016.11.021.
25. C.J. Zou, X.L. Yan, Y.B. Qin, M. Wang and Y. Liu, *Corros. Sci.*, **85**, 445 (2014); https://doi.org/10.1016/j.corsci.2014.04.046.
26. A.A. Farag and M.A. Hegazy, *Corros. Sci.*, **74**, 168 (2013); https://doi.org/10.1016/j.corsci.2013.04.039.
27. Y.S. Fu, H.Q. Chen, X.Q. Sun and X. Wang, *Appl. Catal. B*, **111**, 280 (2012); https://doi.org/10.1016/j.apcatb.2011.10.009.
28. S.C. Yan, Z.S. Li and Z.G. Zou, *Langmuir*, **26**, 3894 (2010); https://doi.org/10.1021/la904023j.
29. T.G. Xu, L.W. Zhang, H.Y. Cheng and Y.F. Zhu, *Appl. Catal. B*, **101**, 382 (2011); https://doi.org/10.1016/j.apcatb.2010.10.007.